

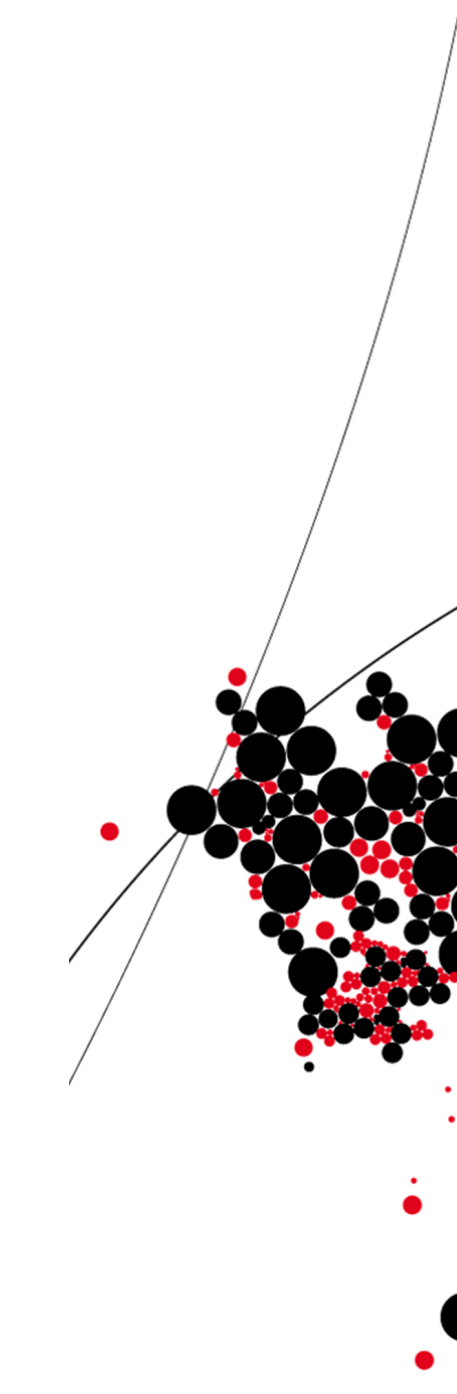


UNIVERSITY OF TWENTE.

**Faculty of Engineering Technology
Department of Biomechanical Engineering**

**Measuring gait characteristics
using wearable sensors in
neurological patients**

**D.J. Cavelaars, BSc
Master Biomedical Engineering
13 October 2023
BE-955**



Graduation committee:
(chair) E. van Asseldonk, dr.
C. Bayón Calderón, dr.
N. Keijsers, dr.
C. Ensink, MSc.
(external member) I. Refai, dr.

CONTENTS

I	Nederlandse samenvatting	2
II	Introduction	3
III	Methods	4
III-A	Participants	4
III-B	Materials	4
III-C	Measurement protocol	4
III-D	Data processing	5
III-E	Algorithms	5
III-E1	Gait events	5
III-E2	Spatiotemporal metrics	6
III-E3	Kinematic metrics	6
III-F	Data analysis	8
IV	Results	8
IV-A	Gait events	8
IV-B	Spatiotemporal metrics	9
IV-C	Kinematic metrics	9
V	Discussion	12
V-A	Gait events	12
V-B	Spatiotemporal and kinematic metrics	13
V-C	Limitations	14
V-D	Recommendations	14
VI	Conclusion	14
	Appendix	16

I. NEDERLANDSE SAMENVATTING

Patiënten ondervinden na een beroerte vaak langdurig last van een pathologische gang vanwege verminderde motorische controle. Gewoonlijk wordt tijdens revalidatie het looppatroon van een patiënt beoordeeld met behulp van een optisch bewegingsopnamesysteem. Dit kan alleen in een gespecialiseerd laboratorium worden uitgevoerd. Het zou nuttig zijn als deze loopkenmerken in een thuissituatie met behulp van draagbare sensoren bepaald zouden kunnen worden. Dit artikel is erop gericht om voor patiënten die na een beroerte geconfronteerd worden met een pathologische gang de loopgebeurtenissen, en tevens de spatiotemporele en kinematische variabelen te bepalen aan de hand van Inertial Measurement Units (IMUs). Een groep van acht patiënten met chronische loopstoornissen, in de leeftijd van 49.0 tot 69.4 jaar zijn geanalyseerd middels IMUs. Een totaal van 8799 passen aan zowel de aangedane als niet-aangedane zijde zijn geanalyseerd. De nauwkeurigheid van voet- en onderbeengebaserde IMU-systemen werden vergeleken met de gouden standaard. Bij het bepalen van loopgebeurtenissen (initial contact, mid-stance, heel-off, terminal contact en mid-swing) aan de aangedane zijde, had het voetgebaseerde systeem een kleinere afwijking (initial contact: 0.01 s; mid-stance: -0.02 s; heel-off: -0.11 s; terminal contact: -0.02 s; mid-swing: 0.02 s) dan het onderbeengebaserde systeem. Tevens had het voetgebaseerde systeem bij de vijf loopgebeurtenissen een kleinere variantie en minder foutgedetecteerde loopgebeurtenissen. Tenslotte is ook de nauwkeurigheid van de spatiotemporele en kinematische variabelen vergeleken tussen de voet- en onderbeengebaserde systemen. De resultaten laten zien dat de voetgebaseerde methode het meest nauwkeurig is voor de meeste variabelen. Concluderend zijn voor patiënten na een beroerte de voetgebaseerde IMUs beter in het bepalen van loopkenmerken dan onderbeengebaserde IMUs.

Measuring gait characteristics using wearable sensors in neurological patients

D.J. Cavelaars, BSc¹

Abstract—Chronic stroke patients often suffer from pathological gait due to decreased motor control. In therapy, a patient’s gait is usually assessed using an optical motion-capturing system, which can only be performed in a specialised lab. It would be beneficial to be able to determine the same gait characteristics at home using wearable sensors. This paper aims to determine gait events, and spatiotemporal and kinematic metrics using Inertial Measurement Units (IMUs) for chronic stroke patients with pathological gait. A group of eight chronic stroke patients aged between 49.0 and 69.4 years were analysed using IMUs. A total of 8799 strides in both affected and unaffected sides were recorded. The accuracy of foot-based and shank-based IMU systems was compared to the gold standard. In detecting gait events (initial contact, mid-stance, heel-off, terminal contact and mid-swing) on the participant’s affected side, the foot-based system had a smaller median error (initial contact: 0.01 s; mid-stance: -0.02 s; heel-off: -0.11 s; terminal contact: -0.02 s; mid-swing: 0.02 s) than the shank-based system. At all five gait events, the foot-based system also had a lower variance and fewer falsely identified gait events. In addition, the accuracy of spatiotemporal and foot kinematic metrics was compared between the foot-based and shank-based systems. The results show that the foot-based gait measurement algorithm is the most accurate for most metrics. In conclusion, foot-based IMUs are better used compared to shank-based IMUs to determine gait characteristics in patients with chronic stroke.

Index Terms—gait analysis; wearable sensors; inertial measurement units; neurological patients; rehabilitation; stroke; pathological gait; GRAIL

II. INTRODUCTION

Stroke is the second leading cause of death and long-term disability worldwide [1]. A stroke (or cerebrovascular accident, CVA) is the interruption of blood flow to parts of the brain. This can either be an ischemic stroke, caused by a blockage of blood vessels, or a hemorrhagic stroke which is caused by the rupture of a blood vessel. About 87% of strokes are ischemic strokes [2]. Long-term disabilities that can result from a stroke include problems with motor control, understanding language, thinking, memory, and sensory and emotional disturbances [3]. The loss of controlled body movements and proper balance often leads to impaired walking abilities [4]. Specifically, a common gait impairment for chronic stroke patients is a decreased strength of the anterior tibialis that can result in a less defined heel strike or even total inability to dorsiflex the ankle. This is called a ‘drop foot’ [5], [6]. A drop foot means that the toes do not clear the ground effectively during the swing phase, increasing

the chances of tripping and decreasing the overall gait stability [4]. Therefore, limiting the drop foot is often a goal in therapy.

The assessment of a patient’s gait is important for clinicians to diagnose and monitor the progress of therapy. The current gold standard for biomechanical assessment of gait is an optical motion-capturing system. Although these systems are very valuable in current clinical practice, measurements can only be performed in a dedicated lab with specialised personnel. In this lab, gait analysis can be performed in a controlled environment, to measure kinetics, kinematics and muscle activity. Not only is gait analysis relevant for monitoring therapy progress, but a real-time gait analysis is essential in the development of novel rehabilitation techniques, such as wearable robotics. An example of these wearable robotics is an assistive ankle-foot orthosis [7], which assists a patient with pathological gait during different gait phases. These assistive devices can be passive, semi-active and active. For the active devices, it is necessary to know in which gait phase the user is in, so that they can adapt their support.

However, there are multiple reasons why it is more advantageous to be able to perform gait analysis in daily life situations rather than in a lab. Patients are no longer required to travel to a specialised lab since physicians can remotely analyse the acquired data, saving time and costs. Laboratory reservations are often limited and restrict the duration of therapy sessions. Moreover, it is more useful to know how patients actually walk during activities of daily living, rather than in a clinical setting under perfect conditions, in order to ensure ecological validity. This could help decide how the gait should be improved in real-world situations where patients encounter various environmental challenges. Furthermore, patients behave differently during measurements in a laboratory environment compared to their daily life [8]. They increase their performance, leading to an overestimation of gait quality.

In the past decades, extensive research has been done on gait analysis with Inertial Measurement Units (IMUs) [9]–[11]. These are wearable sensors and can be deployed in non-standardised settings, opening up the possibility to perform gait analysis in daily life environments. Essential for determining gait characteristics is the accurate detection of gait events, such as terminal contact and initial contact. In normal gait, terminal contact is usually the moment of toe off, while initial contact corresponds with heel strike. An algorithm aiming to determine toe off and heel strike based solely on measurements from foot sensors might not always be possible. A decrease in foot plantar- and dorsiflexion in pathological gait means that initial contact is often not made with the heel, but rather with a flat foot or even the toe, which affects foot-

¹Master student Biomedical Engineering, University of Twente, The Netherlands. Correspondence: d.j.cavelaars@alumnus.utwente.nl

based signal features [9]. These deviating gait patterns and resulting foot-based signal features could lead to the inability to accurately determine gait events based on sensors placed on the feet. Previous work by Behboodi et al. [12] shows an accurate detection of gait events in pathological gait due to cerebral palsy, based on IMUs attached to the shanks. After the gait events are identified, specific gait events can be used to determine the spatiotemporal and kinematic metrics. It is of interest to compare the influence of the different IMU locations on the accuracy of the results, specifically for a group of neurological patients with pathological gait, to investigate whether these are improved with a shank-based system.

The aim of this paper is to determine gait characteristics using wearable sensors for neurological patients with pathological gait. In order to achieve this goal, two sub-questions are formulated: 1) Which IMU location leads to the highest accuracy of gait event detection? 2) What is the accuracy of the spatiotemporal and foot and ankle kinematic metrics, based on gait event detection using IMUs on different locations?

The hypothesis is that shank-based IMU measurements will yield the highest accuracy for gait event detections, compared to foot-based measurements. Based on this hypothesis, it is expected that the spatiotemporal and kinematic metrics also have the highest accuracy when based on IMU measurements from the shank compared to the foot.

III. METHODS

A. Participants

A group of eight stroke patients (age: 62.6 ± 6.7 years, 5 males, 3 females) participated in this study between November 2022 and May 2023. The participant characteristics can be found in Table 1. Participants were recruited online in groups for acquired brain injury sufferers, as well as using connections with physiotherapists in the Nijmegen area, and databases of participants from other studies at the Sint Maartenskliniek who have given permission to be contacted again. The inclusion criteria for the participants of this study were a) at least six months post-stroke, b) the ability to walk without a walking aid for at least five consecutive minutes, c) the ability to understand basic instructions regarding the trials, d) good visual sight to see a display placed in front of the participant, whether or not with correction, and e) at least 18 years of age. In addition to the impairments caused by stroke, the participants had to be free from neurological disorders, lower limb pathologies, and major surgeries which could influence their gait.

Prior to testing, the participants gave their written informed consent in accordance with the Declaration of Helsinki (Version 2013, 04-11-2019). The study was approved by the internal review board of the Sint Maartenskliniek and exempted from the Dutch medical scientific research act (WMO) by the medical ethics board ‘CMO regio Arnhem-Nijmegen’ (identification: 2021-13295). The study was carried out in the Netherlands, in accordance with the Medical Research Involving Human Subjects Act (WMO).

Table 1: Metadata of participants

ID	Sex	Age (years)	Height (cm)	Weight (kg)	Affected side	Stroke type	Years since stroke
pp01	Male	64.3	178	122	Left	Hemorrhagic	15.8
pp02	Female	49.0	171	68	Right	Ischemic	0.7
pp03	Male	61.0	172	75	Right	Unknown	17.5
pp04	Female	57.9	163	70	Left	Ischemic	7.0
pp05	Male	65.2	183	80	Left	Ischemic	0.5
pp06	Male	69.3	194	85	Left	Unknown	1.8
pp07	Male	69.4	183	90	Right	Ischemic	1.5
pp08	Female	64.9	172	91	Right	Hemorrhagic	4.4

B. Materials

The measurements took place in a Gait Real-time Analysis Interactive Lab (GRAIL, Motek Medical, The Netherlands) as shown in Figure 1. During the trials, two separate measurement systems were used simultaneously: a gold standard and a sensor system. The gold standard was an optical motion capture system, measuring at 100 Hz (Vicon, Vicon Motion Systems, United Kingdom) including 20 markers placed according to the plug-in gait lower-limb model [13] (blue dots in Figure 2). The four medial markers (on both knees and ankles) were only used during the calibration of the gold standard and were removed during measurements. The sensor system consisted of five inertial measurement units (IMUs), also measuring at 100 Hz (Xsens MTw Awinda, Movella, The Netherlands). The IMU sensors were placed on the pelvis, shanks and feet (orange rectangles in Figure 2). Data were captured using MT Manager (version 2019.2, Movella, The Netherlands). Both systems were time synchronised by a high-low pulse, with the optical motion capture system as master.



Figure 1: Gait Real-time Analysis Interactive Lab (GRAIL) including the variable-speed treadmill and harness safety hook. The virtual environment and feedback were projected on the screen.

C. Measurement protocol

Each participant performed five trials on the treadmill of the GRAIL, while secured in a harness as a safety precaution, without bodyweight support. Before every trial, instructions were given to the participants, and they were allowed to ask questions and familiarize themselves with the GRAIL.

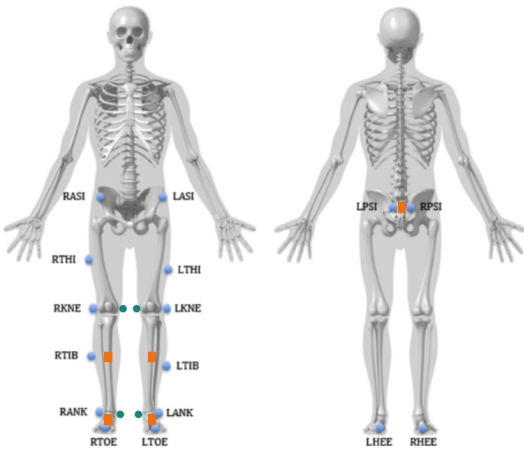


Figure 2: Placement of the markers (blue dots) and IMUs (orange rectangles) on the participants during measurements on the GRAIL (figure adapted from [13]).

environment. Rest breaks in between trials were allowed as much as needed.

Every trial lasted 2-3 minutes, all of which were used for further analysis. The trials took place according to the following scheme:

- 1) self-paced, no feedback
- 2) fixed-pace, feedback A
- 3) fixed-pace, feedback B
- 4) fixed-pace, feedback A + B
- 5) self-paced, no feedback

Participants received real-time feedback based on their gait characteristics during three trials. Feedback A was based on the sagittal foot angle at initial contact, and feedback B on the propulsive force during push-off. During the self-paced trials, the participants could control their own walking speed to a comfortable pace. The participants could increase their speed by moving towards the front of the treadmill and decrease their speed by moving to the back. During the fixed-pace trials, the speed of the treadmill was fixed to the average comfortable walking speed of the first trial.

The feedback was present in order to introduce further variability in the walking patterns within the participants. The order of feedback A and B was randomised between participants. The feedback was based on measurements from the gold standard in real-time. It was presented on a screen of the GRAIL surrounding the participant, with a horizontal bar moving upwards to a green area for an improved metric value, and similarly moving down to a red area for a worsened value. The participants received feedback relative to their own performance at the start of a trial, so they were not competing against other participants. The first ten strides of a trial were used as a baseline, after which the feedback started.

D. Data processing

The optical motion capture data was processed by labelling, gap filling and Woltring filtering [14]. This was done in Nexus, the processing software accompanying Vicon (Nexus version 2, Vicon Motion Systems, United Kingdom). The maximum

gap size that was filled is 50 frames for Rigid Body Filling, and 25 frames for Pattern Filling. Gaps larger than those were left untouched, resulting in no marker data available for those timestamps.

During measurements, the IMU data was automatically filtered to aim for drift-free absolute orientation data. This was done using an Xsens Kalman Filter [15]. The IMU data was saved to a separate `.txt` file for each sensor. It included accelerometer, gyroscope, magnetometer, orientation data (quaternions and Euler angles), and timestamps. These timestamps were synchronised with the five IMUs and the gold standard.

The determination of the gait characteristics and statistical analysis was done in Python (Python version 3.10, Python Software Foundation), with the following packages: SciPy version 1.9.3 [16], Matplotlib version 3.6.3 [17], NumPy version 1.23.5 [18], pyquaternion version 0.9.9 [19].

A second-order low-pass Butterworth filter [20] was used to filter the acceleration ($f_c = 17\text{Hz}$) and gyroscope ($f_c = 15\text{Hz}$) data to remove high-frequency noise. The recursive filter introduced no lag in the signal.

E. Algorithms

1) *Gait events*: The five gait events that were detected are the Initial Contact (IC), Mid-Stance (MSt), Heel-Off (HO), Terminal Contact (TC) and Mid-Swing (MSw), which were detected based on IMU data of the feet or the shanks. Here, three different algorithms are presented. The first is for the foot-based IMU measurements, the second for the shank-based IMU, and lastly for the Vicon system. The IMU algorithms used either the acceleration in z-direction a_z , the angular velocity around the y-axis ω_y , or the absolute angular velocity around the three dimensions $\omega_{x,y,z}$. The axes are in the global frame, as defined in Figure 4. An overview of the signal features used for both feet and shank-based detection is presented in Table 2 and visualised for example gyroscope signal in Figure 6. The definition of the five gait events, along with the gait phases that are of interest in this study, are presented in Figure 3.

a) *Foot-based IMU*: A MSw was determined when the angular velocity of the foot reached a maximum value in the counter-clockwise direction. These peaks were selected with a minimum distance of 0.7 s, and a minimum height of 0.3rad s^{-1} . The IC was defined by the first zero-crossing (positive to negative) of the angular velocity around the y-axis ω_y , after a MSw. The TC was defined by the positive peak in the linear acceleration in the z-direction a_z . In case there were multiple positive peaks, the one with the lowest angular velocity around the y-axis ω_y was selected. The remaining two gait events were based on contralateral events. The MSt was considered the contralateral TC, and the HO was the contralateral MSw.

b) *Shank-based IMU*: The MSw was determined using the angular velocity of the shank around the y-axis ω_y . It was the last zero-crossing (positive to negative) before a maximum peak in the shank angular velocity around the y-axis ω_y . The maximum peaks were determined with a minimum height of

Table 2: The different signal features used for gait event detection, based on two IMU locations

Gait event	Foot-based (a_z or ω_y)	Shank-based (ω_y or $\omega_{x,y,z}$)
Initial contact	Zero-crossing ω_y after mid-swing [12]	IC1: Zero-crossing (negative to positive) ω_y after mid-swing [12] IC2: First negative peak ω_y after maximum peak ω_y
Mid-stance	Contralateral terminal contact [21]	Contralateral terminal contact [21]
Heel-off	Contralateral mid-swing [12]	Contralateral mid-swing [12]
Terminal contact	Peak a_z [22]	TC1: Positive peak absolute value of $\omega_{x,y,z}$ TC2: Last negative peak ω_y before maximum peak ω_y
Mid-swing	Peak ω_y [20]	Zero-crossing (positive to negative) ω_y [12]

1 rads^{-1} , and a minimum distance between them of 0.5 s. The IC and TC had two different algorithms that are based on shank measurements. The first algorithm for IC (named IC1) considered the first zero-crossing (negative to positive) of the shank angular velocity around the y-axis ω_y , after MSw. The first algorithm for TC (named TC1) looked at the last positive peak of the shank angular velocity (sum of all three gyroscope dimensions, $\omega_{x,y,z}$), after MSw. The second algorithms for IC and TC (named IC2 and TC2 respectively) looked at the local minima between two maxima in the shank angular velocity around the y-axis ω_y . The maximum peaks were determined in the same way as for MSw. Between these maximum peaks, the minima were found with a distance of at least 0.25 s. The first minimum corresponded to IC2, and the last minimum to TC2. The MSt and HO events were determined in the same way as the foot-based system, namely using the contralateral gait events of TC and MSw, respectively.

c) *Vicon*: For the gold standard, the IC and TC events were determined using the velocity-based treadmill algorithms by Zeni et al. [23]. The MSw was defined as the mid-point in time between the TC and IC. The MSt was defined as the contralateral TC. The HO was the moment when the heel marker rose 1 cm above its mean value during the flat foot phase for at least 0.1 s.

2) *Spatiotemporal metrics*: The definitions of spatiotemporal and kinematic metrics are reported in Table 3, for both the sensor system and the gold standard.

Most spatiotemporal metrics can be directly calculated as being a duration between multiple gait events. The difference in timestamps is used to determine these metrics. However, for the peak angular velocity, stride length, stride velocity and asymmetry indices, a distance or velocity is required. These are calculated for every stride.

For the IMU system, the velocity v in the walking direction was calculated by numerically integrating the acceleration a_x data (Equation 1). This is the acceleration in the global frame, in the walking direction. The position d was calculated in the same way using the velocity (Equation 2). The initial values of the velocity and position are set to zero ($v_0 = 0 \text{ms}^{-1}$ and $d_0 = 0\text{m}$), because the treadmill was stationary at the start of every trial.

$$v_i = v_{i-1} + a_i / f_s \quad (1)$$

$$d_i = d_{i-1} + v_i / f_s \quad (2)$$

The asymmetry index (ASI) is a measure to compare the symmetry between metrics on both sides. It was calculated using Equation 3, for both the stride time and stride length. In calculating the ASI, the mean value per trial of the affected side (μ_A) was compared to the unaffected side (μ_U). An ASI of 0% represents perfect symmetry between the affected and unaffected sides. A positive ASI means that the metric of the affected side had a larger mean value during a trial, and similarly, a negative ASI means that the metric of the affected side had a smaller mean value.

$$ASI(\mu_A, \mu_U) = \frac{2(\mu_A - \mu_U)}{\mu_A + \mu_U} \cdot 100\% \quad (3)$$

The metrics of the gold standard were compared with those of the sensor system. It is vital that the outcome of the IMU-based metric is compared to the metric of the same stride of the gold standard. Therefore, the metrics were only compared to each other if they fell within a 0.5-second window of each other. If no corresponding metric was found within this window, it was assumed that the IMU system identified a stride when there actually was not (false positive), or the IMU system did not identify a stride when there actually was one (false negative). It was not always possible to determine reliable gait events for the gold standard. Obvious errors in gait event detection by the gold standard due to missing markers were omitted before further analysis.

3) *Kinematic metrics*: To determine the foot and ankle angle metrics, the position and (relative) orientation of the shank and foot segments must be known. The IMUs were attached to the body segments but were not perfectly aligned with them. The actual orientations of the IMUs were of little interest, instead, the orientations of the body segments are. For every body segment, a body segment frame was created, from which the (relative) orientation could be calculated. Next to that, the body segment frame could be expressed with respect to the global frame.

The body segment frames of the setup are shown in Figure 4. The orientation of the sensor frame of the Xsens Awinda can be found in Figure 5.

Generally, quaternions can be used to express the rotation from one frame to another. Quaternions were used instead of Euler angles because they do not have the problem of a gimbal lock, making them more robust during calculations. Here, a quaternion was used to express the rotation between an IMU frame to a body segment frame. From this, a quaternion of the body frame (*BF*) with respect to the global frame (*GF*) was

Table 3: The definitions of all output variables

Output variables	Unit	Definition
Cycle duration	s	duration from initial contact to initial contact
Cadence	cycles/s	number of strides per second
Stance duration	% gait cycle	duration from initial contact to terminal contact, as a percentage of cycle duration
Swing duration	% gait cycle	duration from terminal contact to initial contact, as a percentage of cycle duration
Push-off duration	% stance duration	duration from heel-off to toe-off, as a percentage of stance duration
Double support duration	% gait cycle	combined duration from right initial contact to left terminal contact, and left initial contact to right terminal contact, as a percentage of cycle duration
Stride length	m	distance covered between terminal contact and initial contact
Stride velocity	m/s	stride length divided by cycle duration
Peak angular velocity	deg/s	maximum shank angular velocity during swing phase
Asymmetry index	left/right %	using cycle duration and stride length in Equation 3
Foot angle	deg	angle between foot and ground (dorsiflexion is positive) at IC, MSt and TC

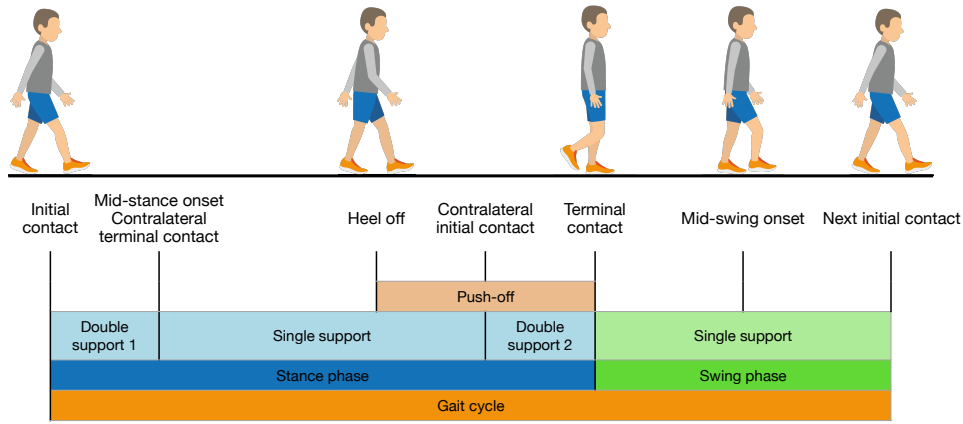


Figure 3: Typical gait cycle with gait events (adapted from burorub / SMK Research).

calculated. Quaternions have the general form of Equation 4:

$${}^{GF} \mathbf{q}_{BF} = a + b\mathbf{i} + c\mathbf{j} + d\mathbf{k} = [a \ b \ c \ d] \quad (4)$$

Here, a , b , c and d are real numbers and represent the magnitude of the basis vectors (\mathbf{i} , \mathbf{j} and \mathbf{k}).

The body segment frames were described as quaternion rotations, based on their initial position during calibration, where the participant was assumed to be standing in an upright position as in Figure 4. Table 4 shows the initial quaternion definitions for the three segments, based on the method from Vargas-Valencia [24]. The pelvis frame was aligned with gravity, from which the other frames are calculated. These body segment frames are presented schematically in Figure 4.

Table 4: Definition of technical-anatomical

Segment	Initial Quaternion Definition
Pelvis (PV)	${}^{GF} \mathbf{q}_{BF-PV_0}$
Shank (SH)	${}^{GF} \mathbf{q}_{BF-SH_0} = {}^{GF} \mathbf{q}_{BF-PV_0} \otimes \mathbf{q}_{ROT}(180^\circ, \mathbf{i})$
Foot (FT)	${}^{GF} \mathbf{q}_{BF-FT_0} = {}^{GF} \mathbf{q}_{BF-SH_0} \otimes \mathbf{q}_{ROT}(90^\circ, \mathbf{j})$

Where $\mathbf{i} = [1 \ 0 \ 0]^T$, $\mathbf{j} = [0 \ 1 \ 0]^T$, and $\mathbf{q}_{ROT}(\theta, \mathbf{n})$ is the quaternion of rotation as defined in Equation 5:

$$\mathbf{q}_{ROT}(\theta, \mathbf{n}) = \left[\cos\left(\frac{\theta}{2}\right) \quad \mathbf{n} \sin\left(\frac{\theta}{2}\right) \right] \quad (5)$$

Lastly, the IMU frame could be rotated to the corresponding body frame for a certain segment B using Equation 6:

$${}^{BF-B} \mathbf{q}_{IMU-F-B} = {}^{GF} \mathbf{q}_{BF-B_0}^* \otimes {}^{GF} \mathbf{q}_{IMU-F-B} \quad (6)$$

Most of the quaternion calculations were done using the SciPy package. This also allows for conversion from quaternion to Euler angles, which was used for the end results of the foot and ankle angles. The Euler angles for pitch, roll and yaw represent the dorsiflexion-plantarflexion, medial-lateral rotation and inversion-eversion of the foot respectively.

The foot angle θ_{foot} was defined as the Euler angle around the y-axis between the foot body frame and the global frame ${}^{GF} \mathbf{q}_{BF-FT}$.

The ankle angle θ_{ank} was defined as the angle between the shank \mathbf{q}_{SH} and foot \mathbf{q}_{FT} body frames using Equation 7:

$$\theta_{ank} = \arccos \frac{\mathbf{q}_{SH} \cdot \mathbf{q}_{FT}}{\|\mathbf{q}_{SH}\|_2 \|\mathbf{q}_{FT}\|_2} \quad (7)$$

To accommodate for the signal drift present in the IMU foot angle, the foot angle was reset to an angle of zero degrees at every MSt.

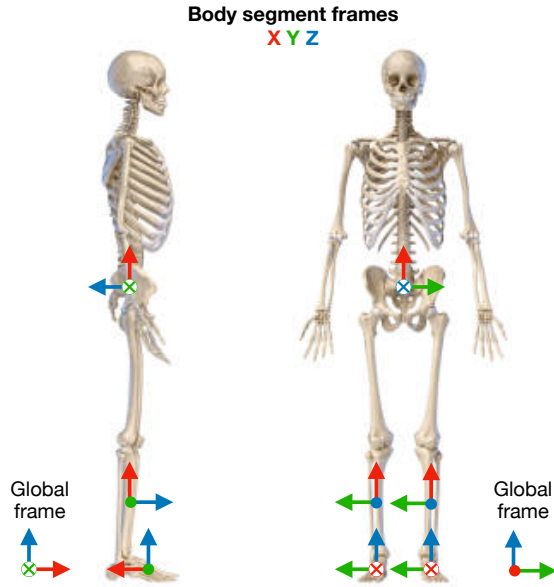


Figure 4: Right-handed coordinate frames of the global frame and body segment frames of the IMU setup. The x-axis of the global frame is pointing in the walking direction. The IMUs were mounted on the pelvis, shanks and feet. The x-axes are represented in red, y-axes in green and z-axes in blue. A dot is an arrow coming towards the reader, and a cross is an arrow pointing away.

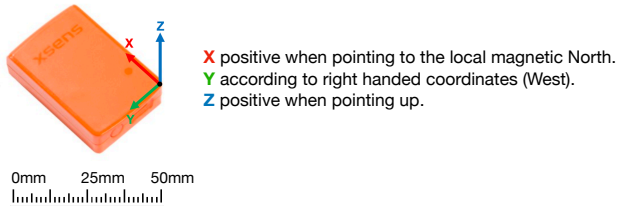


Figure 5: Sensor frame of the Xsens Awinda IMU [25].

F. Data analysis

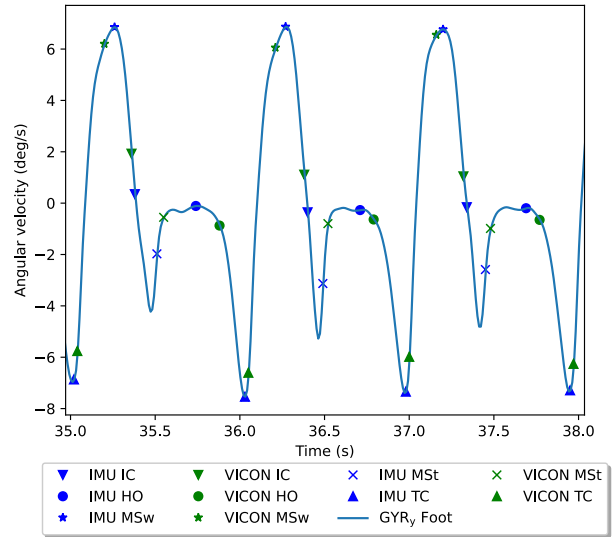
The results of the two IMU systems were compared to the gold standard. For the gait event detections, the errors between the two systems were compiled in box plots. Here, the median and variance in error, and the number of false detections are considered when choosing an optimal system.

For the spatiotemporal and kinematic metrics, the comparison was done using Bland-Atlman plots [26]. These visualise the mean difference between the gold standard and the sensor system, and the 95% limits of agreement (1.96 times the standard deviation of the difference). To quantify these results, both the mean and standard deviation of the error (i.e. accuracy and precision) are considered. These results were expressed as absolute errors, and as a percentage with respect to the mean value of the gold standard.

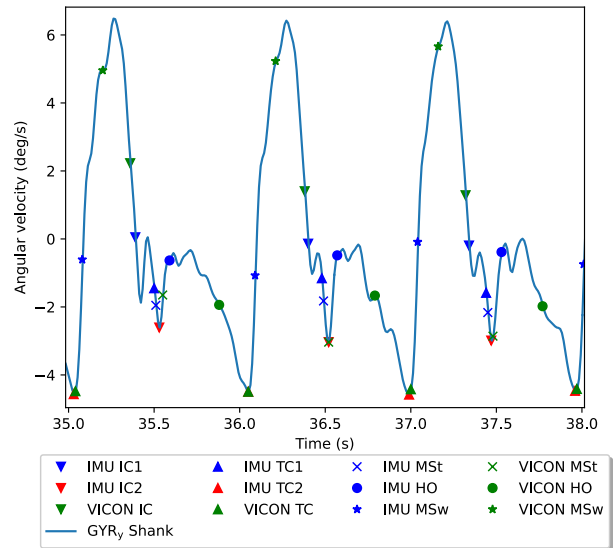
IV. RESULTS

A. Gait events

First, the gait events were determined according to the algorithms in Table 2. A total of 4415 strides were recorded



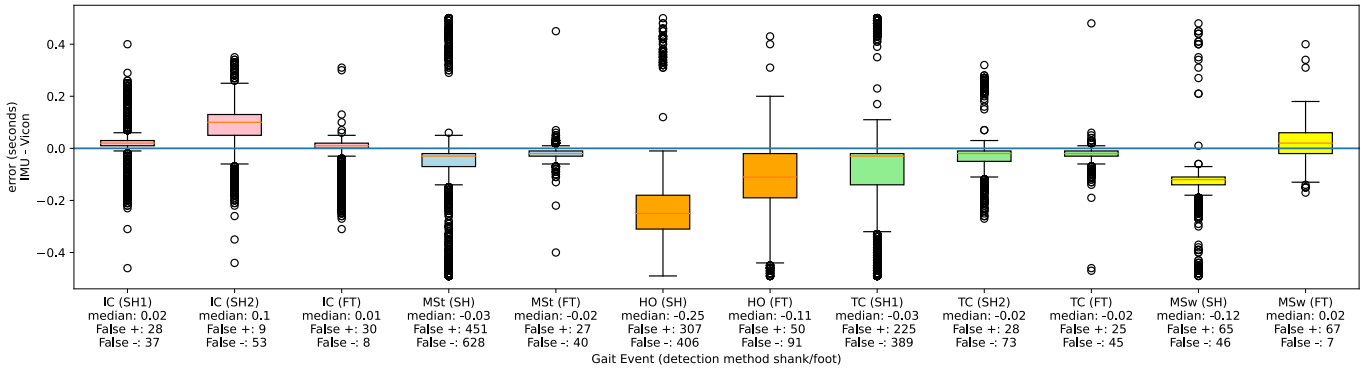
(a) Foot gyroscope data of affected side.



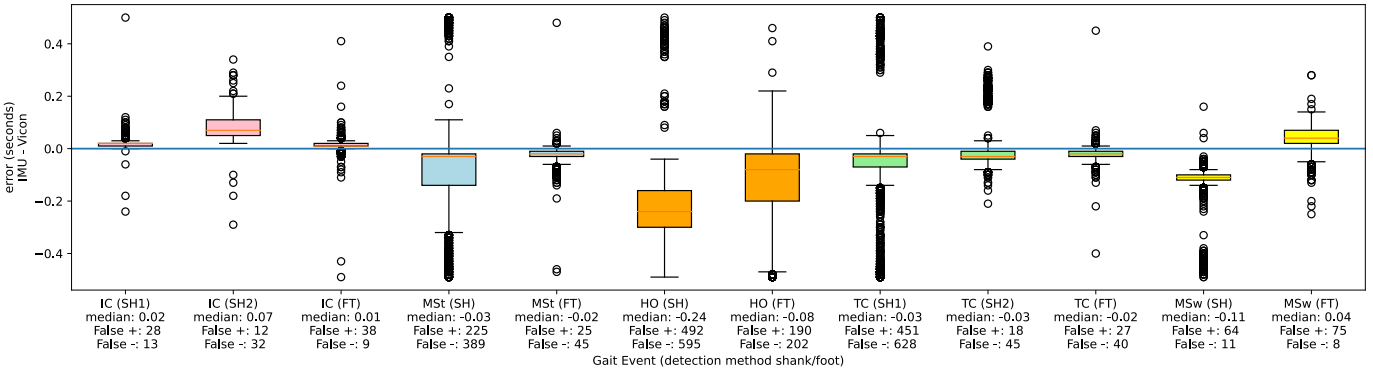
(b) Shank gyroscope data of affected side. For the IC and TC, there are two different detection algorithms for the IMU system.

Figure 6: Time series of filtered foot (panel A) and shank (panel B) gyroscope data around the y-axis of a representative trial. The five different gait events are determined by the IMU and Vicon systems separately, but plotted in the same figure to visualise the detection methods and inaccuracies. In the first panel, foot-based detection is applied, and in the second panel, shank-based detection is used.

and analysed on the affected side of the participants, and 4406 on the unaffected side. The signals shown in Figure 6 are of a representative walking pattern of the participants. The top panel A shows the gait event detection for the algorithm based on the IMUs placed on the feet, while the bottom panel B shows the gait event detection for both algorithms based on the IMUs placed on the shanks. For the foot-based detections, the MSt, HO and TC events are mostly too early compared to the gold standard. The IC and MSw are detected too late.



(a) Box plots for affected sides.



(b) Box plots for unaffected sides.

Figure 7: Box plot of gait event detection errors of all participants combined, for the five gait events. There are two shank algorithms per IC and TC. The median and number of false positives and false negatives are declared below each box. The height of the box represents the interquartile range.

In this figure, there are no false positive or false negative detections visible. For the shank-based system, the two IC algorithms are both too late (IC2 later than IC1). The MSt, HO and Msw are too early compared to the gold standard. The first TC algorithm (TC1) is shifted about half a stride from the gold standard, because a wrong minimum is being detected. TC2, however, is very close to the gold standard but has false negative detections (i.e. not all events are recognised).

The error compared to the gold standard is calculated for every gait event detection method. At all five gait events, the median error and total number of false detections are the smallest for the foot-based algorithm on the affected side. However, there are slight differences for the unaffected side. At IC, TC and Msw, the median error is lowest for the foot-based system, whereas the shank algorithm has a slightly lower number of false detections for IC1 and TC2. The results are plotted as box plots in Figure 7 separately for the affected and unaffected side. Here, the trials of all participants are combined, considering their respective affected sides.

B. Spatiotemporal metrics

For the spatiotemporal and kinematic metrics, a total of 8799 strides were analysed at the affected and unaffected sides combined. For the shank algorithms, the gait events of IC1 and TC2 were used, due to their highest accuracy for the gait events.

These results show that for most spatiotemporal metrics, the foot-based gait event detection yields the lowest mean and standard deviation of the error. However, the swing duration has a lower mean and standard deviation with the shank-based system. The stance duration for the shank-based system has a lower mean error, but a higher standard deviation. For the peak angular velocity, the results are equal between the foot-based and shank-based systems. The results of the spatiotemporal metrics are represented as Bland-Altman plots in Figure 8 for the foot-based detections, and in Figure 9 for the shank-based detections. The mean and standard deviation of the differences are presented in Table 5.

A positive mean error in a Bland-Altman plot represents an overestimation of the IMU-derived metric, and similarly, a negative mean error means an underestimation by the IMU metric. All metrics except push-off duration, have the same sign for the mean error in the Bland-Altman plots of the foot-based and shank-based systems.

C. Kinematic metrics

The kinematic variables of interest in this study are the foot angles at IC, MSt and TC. Figure 10 shows a representative foot angle over five gait cycles. Here the IMU foot angle signal has a similar shape and amplitude compared to the gold standard.

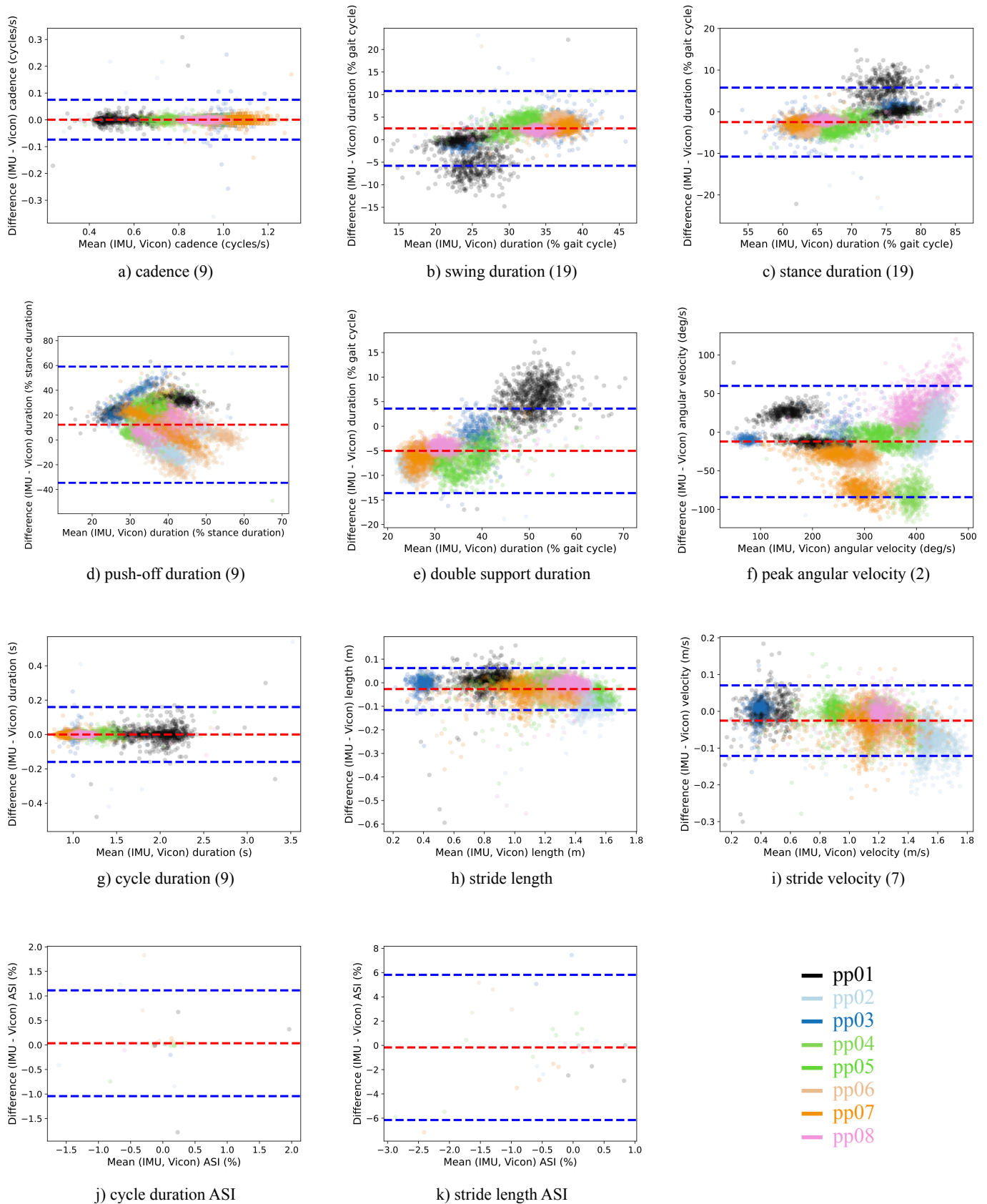


Figure 8: Bland-Altman plots for spatiotemporal metrics of all participants, for the foot-based IMU system. The results from all participants and both sides (affected and unaffected) are combined in a single plot per metric, but visualised in a different color per participant. Some outliers have been omitted from representation in the plot, but are still used for the calculation of the statistics. The number of samples left out is in parentheses below the figures. The red line is the mean difference between the gold standard and the sensor system, and the blue lines represent the 95% limits of agreement (1.96 times the standard deviation of the difference). The two ASI metrics have substantially fewer data points because only one value is determined per trial. The other metrics yield a data point for each stride.

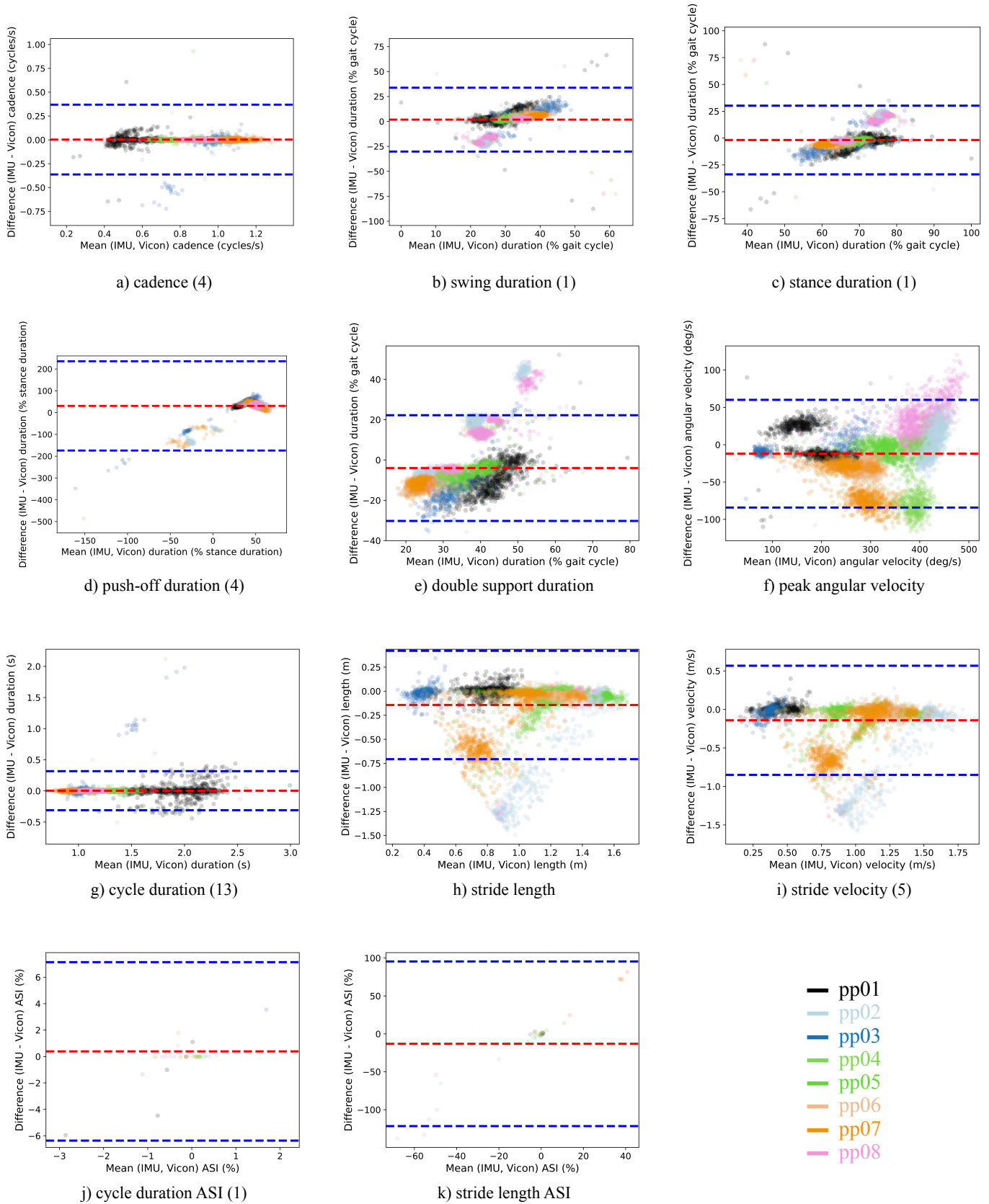


Figure 9: Bland-Altman plots for spatiotemporal metrics of all participants, for the shank-based IMU system (number of samples omitted from figure in parentheses). For IC, the first shank algorithm was used (IC1), and for TC, the second was used (TC2).

Table 5: Results from Bland-Altman plots. Error as a percentage relative to the mean value of the gold standard, and as absolute values. Results for both the foot-based and shank-based system.

Metric	Relative mean \pm std error		Absolute mean \pm std error		Unit
	Foot-based event detection	Shank-based event detection	Foot-based event detection	Shank-based event detection	
Cycle duration	0.0 % \pm 7.0 %	0.0 % \pm 13.9 %	0.00 \pm 0.08	0.00 \pm 0.16	s
Cadence	0.0 % \pm 4.4 %	0.0 % \pm 20.8 %	0.00 \pm 0.04	0.00 \pm 0.19	cycles/s
Stance duration	-3.7 % \pm 6.2 %	-2.7 % \pm 24.2 %	-2.5 \pm 4.2	-1.8 \pm 16.3	% gait cycle
Swing duration	37.4 % \pm 73.2 %	5.5 % \pm 49.9 %	2.5 \pm 4.2	1.8 \pm 16.3	% gait cycle
Push-off duration	-15.8 % \pm 13.9 %	97.2 % \pm 330.7 %	12.2 \pm 23.9	30.7 \pm 104.5	% stance duration
Double support duration	-0.1 % \pm 0.1 %	-11.5 % \pm 38.6 %	-5.0 \pm 4.4	-4.0 \pm 13.4	% gait cycle
Stride length	-2.4 % \pm 4.0 %	-12.3 % \pm 25.5 %	-0.027 \pm 0.046	-0.14 \pm 0.29	m
Stride velocity	-2.4 % \pm 4.7 %	-13.3 % \pm 34.3 %	-0.025 \pm 0.049	-0.14 \pm 0.36	m/s
Peak angular velocity	-3.7 % \pm 11.2 %	-3.7 % \pm 11.2 %	-12.1 \pm 36.8	-12.1 \pm 36.8	deg/s
Stride length ASI	-25.9 % \pm 472.8 %	-1998.1 % \pm 8449.9 %	-0.17 \pm 3.1	-13.1 \pm 55.4	%
Cycle duration ASI	91.2 % \pm 1433.2 %	1016.3 % \pm 8860.1 %	0.035 \pm 0.55	0.39 \pm 3.4	%
Foot angle at IC	-52.4 % \pm 65.1 %	-1.8 % \pm 125.3 %	-12.8 \pm 15.9	-0.45 \pm 30.6	deg
Foot angle at MSt	-99.9 % \pm 148.6 %	-79.4 % \pm 589.3 %	-3.9 \pm 5.8	-3.1 \pm 23.0	deg
Foot angle at TC	-35.2 % \pm -58.5 %	-71.2 % \pm -71.6 %	18.3 \pm 30.4	37.0 \pm 37.2	deg

The Bland-Altman plots following from the results for all participants combined are shown in Figure 11 for the foot-based and shank-based systems. The mean and standard deviation of the error are in Table 5. These errors are generally large, relative to the value of the gold standard. The foot angles at IC and MSt have a smaller mean error for the shank-based system, but a larger standard deviation. At TC, the foot angles for the foot-based system have smaller values for both the mean and standard deviation of the error.

The foot angles at the shank-based gait events show a positive linear relationship between the difference and mean value of the IMU system and the gold standard. The foot-based results at MSt show a negative linear relationship.

V. DISCUSSION

In this study, a group of chronic stroke patients participated in collecting treadmill data using a gold standard and an IMU system. The goal was to investigate which IMU location leads to the highest accuracy in gait event detections. Subsequently, the accuracy of the spatiotemporal and kinematic metrics that follow from the gait events are investigated.

A. Gait events

In contrary to what was expected in the hypothesis, for these pathological gait patients the foot-based algorithms produce the highest accuracy in gait event detection compared to shank-based detection. For most metrics, the median error is only one or two frames (at 100Hz). The HO has a larger error of 11 frames. The minimum detectable timing for gait events with this system is 10 ms. This would seem useful for clinical purposes, but there is still a rather large variance in the data. Therefore the results are not very precise and might not be applicable in a clinical setting depending on the requirements.

The gait events were paired between the IMU and Vicon system with a window of 0.5 s. Decreasing this window would mean that the errors in the box plots would decrease as well, since only the most accurate detections would be included in the analysis. However, this would not be a fair representation of the actual system. The event pairing is meant to correlate the correct strides with each other, but not to increase its accuracy. Moreover, decreasing the window size would also increase the number of false positive and false negative detections. The large number of false positive detections by the IMU system is sometimes due to Vicon wrongly missing gait events, so the IMU system could be performing better than is concluded with this measurement method.

If a gait event is missing for one of the systems, then the spatiotemporal metric for that stride would be too large, since

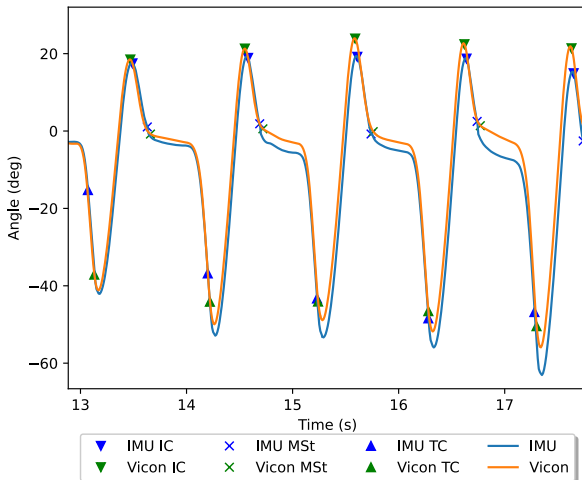
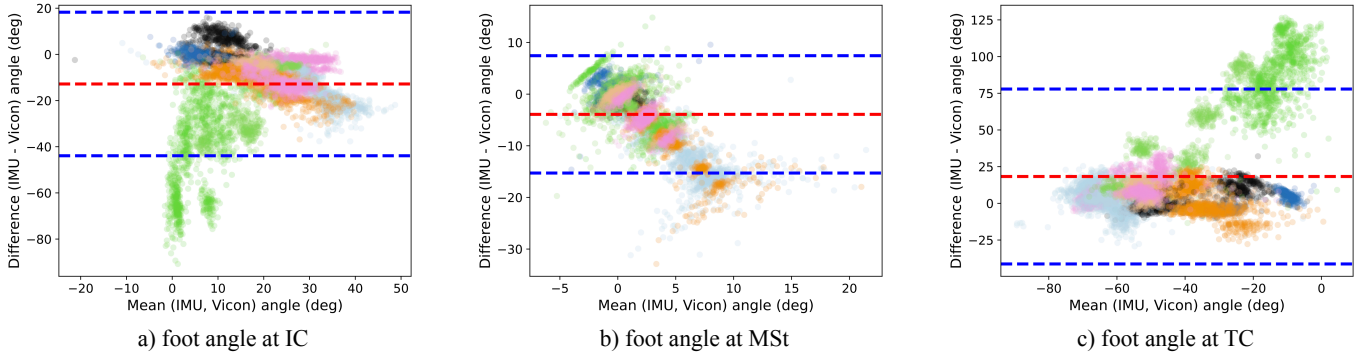
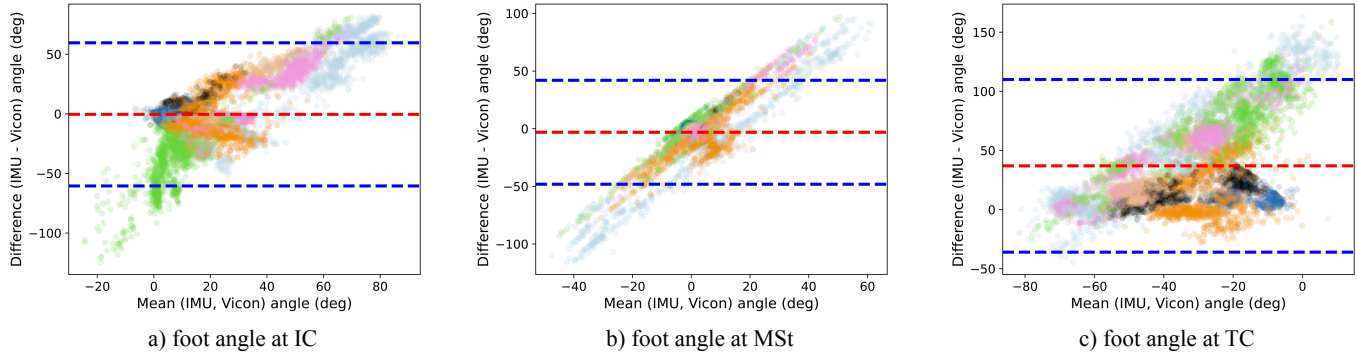


Figure 10: Foot angles of a representative trial, measured with IMU and Vicon system. The respective gait events are marked on the foot angles.



(a) Bland-Altman plots for the foot-based IMU system.



(b) Bland-Altman plots for the shank-based IMU system.

Figure 11: Bland-Altman plots for kinematic variables of all participants, for both foot-based and shank-based IMU systems. Each participant is visualised in the same colors as in Figures 8 and 9.

the algorithm is measuring up to the subsequent gait event that is available. This gives an overestimation of the resulting metric.

Some gait event detections have a large error between the sensor system and the gold standard. This is because the algorithm detects a wrong signal feature. The gyroscope and acceleration signals have multiple maxima, minima and zero-crossings per gait cycle. These features are required for the gait event detection. If a wrong feature is detected, the error in timing can be quite large.

B. Spatiotemporal and kinematic metrics

When considering both the accuracy and precision, the results show that for most spatiotemporal metrics, the foot-based gait event detection performs best. Despite having a relatively accurate gait event detection, the resulting spatiotemporal and kinematic metrics are not always accurate. These metrics often combine multiple gait events to get a result (such as push-off duration), which means that the variance in the data accumulates in the error. The metrics that depend on only one type of gait event, such as IC and the subsequent IC for cycle duration, have a higher accuracy than when combining multiple gait events, such as IC and TC for stance duration.

We can clearly see that the results in the Bland-Altman plots are clustered per participant, where sometimes it is also possible to see the variations within the different trials. The

participants performed differently, but there does not seem to be an outlying participant that has larger errors than the others based on this representation. Even though participant pp05 does deviate from the others for the foot angle at IC and TC for the foot-based algorithm, the choice was made to keep all participants in the analysis.

For the foot angles, a small deviation in the timing of the specific gait events has a large effect on the resulting angle. The foot angle is generally at the maximum value around IC and the minimum around TC. There are steep slopes at both points in the signal, meaning that a small discrepancy in timing of IC or TC events then results in a relatively large angle error.

Although the foot angle is reset to zero degrees at every MSt, the error between the two systems is not zero. This is because the drift correction is done after the measurement has been recorded. The results shown are the values taken before they were reset to zero degrees.

In Table 5, the results from the Bland-Altman plots are presented. Here, it can be seen that the relative error of the asymmetry indices are large. This is because the absolute value of the gold standard is close to zero.

Even though the foot-based system results in the highest accuracy for the gait event detection and metric estimation, other factors should not be ignored. If measurements with the sensor system are performed at home without professional help, then it is important that the setup process is kept as

simple as possible. Perhaps for severely affected chronic stroke patients, it is too difficult to attach IMU sensors to the feet, but still possible to attach them to the shanks. There is, however, a substantial gain in accuracy and precision by having the IMUs on the feet. Moreover, some metrics such as foot angle are not possible to be determined by solely having shank sensors. Therefore it is best to implement a foot-based IMU system.

Moreover, if measurements are done with the proposed sensor system, the other valuable qualities of a gait analysis lab are ignored, such as the kinetic and muscle activity measures. These have not been included in this study.

C. Limitations

Even though the Vicon system used during the experimental phase is considered a gold standard, its analysis following the measurements is not standardised. The implementation of the gait event detection algorithms by Zeni et al. [23] is not fixed, and left some room to tune some parameters such as thresholds based on the data. This meant that the resulting metrics were not always reliable. When there were obvious errors in the Vicon system, they were omitted from the analysis. Obvious errors that were removed are negative values where only positive values are possible, or infinite values. These only minimally affected the results, because they were fully left out from analysis. This meant that the value of the IMU system was not considered at all. Moreover, sometimes it was not possible to determine a metric for the Vicon system, due to missing optical markers.

A limitation of this study is that no other neurological patients were included, such as cerebral palsy patients. Currently only chronic stroke patients were included. It would be of interest to apply the same method to this broader group and investigate the results. These different neurological patients have different pathologies, which means that certain signal features might not be able to be used to detect gait events. Having a system that works for a broader population with different pathologies is a valuable asset in clinical use.

Another limitation of this system is that it only works on a horizontal ground surface since the foot angle at MSt is reset to zero degrees at every stride, to compensate for the drift. Moreover, the analysis does not work in real-time. Some algorithms for the gait event detections use signal features of the future to determine events in the past. If real-time analysis is required, a different digital filter is necessary. Moreover, the shank-based algorithms for MSw, TC1, IC2 and TC2 will have to work differently since they looked at signal features in the future.

D. Recommendations

Sometimes it was difficult to determine the parameters of Python functions, such as minimum peak height or peak distance, that were applicable to all trials of all participants in the IMU system. Perhaps machine learning could optimise these tuneable parameters. A recommendation for new research could be to attempt to implement this in the same algorithms, so their accuracy are improved. Furthermore, it would be interesting to investigate whether machine learning

could fully detect gait events independently, without using the traditional methods as presented in this article. When training a machine learning model, it would be of importance to only train it based on a smaller part of the entire dataset, such that the model does not become over-fitted. It could then be researched whether that model is applicable to the rest of the population.

VI. CONCLUSION

Gait characteristics have been determined using IMU wearable sensors. To answer the first research sub-question, the IMU location that yields the most accurate gait event detections is the feet. Foot-based measurements have the smallest median error and number of false detections compared to shank-based measurements, for the affected side and for all five studied gait events. The second sub-question investigates the accuracy of the spatiotemporal and kinematic metrics that follow from the gait event detection. For most metrics (apart from swing and stance duration), the foot-based measurements have a higher accuracy and precision compared to the shank-based. The foot angles do not have a high accuracy. Metrics that rely on a single type of gait event produce results with higher accuracy than those combining multiple gait events.

ACKNOWLEDGEMENT

The author gratefully thanks the help and support by the supervisors at the University of Twente and Sint Maartenskliniek. They are E. van Asseldonk, C. Bayón Calderón, I. Refai, N. Keijsers, C. Ensink, and C. Hofstad. They assisted during every phase of this study, from helping during participant recruitment and measurements, to giving valuable feedback for the analysis and writing.

CONFLICTS OF INTEREST

The author declares no conflict of interest.

REFERENCES

- [1] V. Saini, L. Guada, and D. R. Yavagal, “Global epidemiology of stroke and access to acute ischemic stroke interventions,” *Neurology*, vol. 97, no. 20 Supplement 2, S6–S16, Nov. 2021. DOI: 10.1212/wnl.0000000000012781. [Online]. Available: <https://doi.org/10.1212/wnl.0000000000012781>.
- [2] C. W. Tsao, A. W. Aday, Z. I. Almarzooq, *et al.*, “Heart disease and stroke statistics—2022 update: A report from the american heart association,” *Circulation*, vol. 145, no. 8, Feb. 2022. DOI: 10.1161/cir.000000000001052. [Online]. Available: <https://doi.org/10.1161/cir.000000000001052>.
- [3] NINDS, *Post-stroke rehabilitation*, 2020. [Online]. Available: <https://www.stroke.nih.gov/materials/rehabilitation.htm>.
- [4] K. K. Karunakaran, R. Pilkar, N. Ehrenberg, K. S. Bentley, J. Cheng, and K. J. Nolan, “Kinematic and functional gait changes after the utilization of a foot drop stimulator in pediatrics,” *Frontiers in Neuroscience*, vol. 13, Jul. 2019. DOI: 10.3389/fnins.2019.00732. [Online]. Available: <https://doi.org/10.3389/fnins.2019.00732>.
- [5] ProtoKinetics, *Common gait deviations: Post-stroke hemiplegic gait*, 2021. [Online]. Available: <https://www.protokinetics.com/common-gait-deviations-post-stroke-hemiplegic-gait/>.
- [6] F. Berenpas, A. Geurts, N. Keijsers, and V. Weerdesteijn, “Benefits of implanted peroneal functional electrical stimulation for continual gait adaptations in people with ‘drop foot’ due to chronic stroke,” *Human Movement Science*, vol. 83, p. 102953, Jun. 2022. DOI: 10.1016/j.humov.2022.102953. [Online]. Available: <https://doi.org/10.1016/j.humov.2022.102953>.
- [7] J. S. Lora-Millan, M. Nabipour, E. van Asseldonk, and C. Bayón, “Advances on mechanical designs for assistive ankle-foot orthoses,” *Frontiers in Bioengineering and Biotechnology*, vol. 11, Jul. 2023. DOI: 10.3389/fbioe.2023.1188685. [Online]. Available: <https://doi.org/10.3389/fbioe.2023.1188685>.
- [8] V. V. Shah, J. McNames, M. Mancini, *et al.*, “Laboratory versus daily life gait characteristics in patients with multiple sclerosis, parkinson’s disease, and matched controls,” *Journal of NeuroEngineering and Rehabilitation*, vol. 17, no. 1, Dec. 2020. DOI: 10.1186/s12984-020-00781-4. [Online]. Available: <https://doi.org/10.1186/s12984-020-00781-4>.
- [9] H. Prasanth, M. Caban, U. Keller, *et al.*, “Wearable sensor-based real-time gait detection: A systematic review,” *Sensors*, vol. 21, no. 8, p. 2727, Apr. 2021. DOI: 10.3390/s21082727. [Online]. Available: <https://doi.org/10.3390/s21082727>.
- [10] C. Gu, W. Lin, X. He, L. Zhang, and M. Zhang, “IMU-based motion capture system for rehabilitation applications: A systematic review,” *Biomimetic Intelligence and Robotics*, vol. 3, no. 2, p. 100097, Jun. 2023. DOI: 10.1016/j.birob.2023.100097. [Online]. Available: <https://doi.org/10.1016/j.birob.2023.100097>.
- [11] G. P. Panebianco, M. C. Bisi, R. Stagni, and S. Fantozzi, “Analysis of the performance of 17 algorithms from a systematic review: Influence of sensor position, analysed variable and computational approach in gait timing estimation from IMU measurements,” *Gait & Posture*, vol. 66, pp. 76–82, Oct. 2018. DOI: 10.1016/j.gaitpost.2018.08.025. [Online]. Available: <https://doi.org/10.1016/j.gaitpost.2018.08.025>.
- [12] A. Behboodi, N. Zahradka, H. Wright, J. Alesi, and S. C. K. Lee, “Real-time detection of seven phases of gait in children with cerebral palsy using two gyroscopes,” *Sensors*, vol. 19, no. 11, p. 2517, Jun. 2019. DOI: 10.3390/s19112517. [Online]. Available: <https://doi.org/10.3390/s19112517>.
- [13] C-Motion, *Tutorial: Plug-in gait lower-limb*, 2022. [Online]. Available: https://www.c-motion.com/v3dwiki/index.php/Tutorial:_Plug-In_Gait_Lower-Limb.
- [14] H. J. Woltring, “A fortran package for generalized, cross-validatorspline smoothing and differentiation,” *Advances in Engineering Software (1978)*, vol. 8, no. 2, pp. 104–113, Apr. 1986. DOI: 10.1016/0141-1195(86)90098-7. [Online]. Available: [https://doi.org/10.1016/0141-1195\(86\)90098-7](https://doi.org/10.1016/0141-1195(86)90098-7).
- [15] M. P. *et al.*, *Xsens mtw awinda: Miniature wireless inertial-magnetic motion tracker for highly accurate 3d kinematic applications*, Accessed: 9-1-2023. [Online]. Available: https://www.xsens.com/hubfs/3446270/Downloads/Manuals/MTwAwinda_WhitePaper.pdf.
- [16] P. Virtanen, R. Gommers, T. E. Oliphant, *et al.*, “SciPy 1.0: Fundamental Algorithms for Scientific Computing in Python,” *Nature Methods*, vol. 17, pp. 261–272, 2020. DOI: 10.1038/s41592-019-0686-2.
- [17] J. D. Hunter, “Matplotlib: A 2d graphics environment,” *Computing in Science & Engineering*, vol. 9, no. 3, pp. 90–95, 2007. DOI: 10.1109/MCSE.2007.55.
- [18] C. R. Harris, K. J. Millman, S. J. van der Walt, *et al.*, “Array programming with NumPy,” *Nature*, vol. 585, no. 7825, pp. 357–362, Sep. 2020. DOI: 10.1038/s41586-020-2649-2. [Online]. Available: <https://doi.org/10.1038/s41586-020-2649-2>.
- [19] K. Wynn, Oct. 2020. [Online]. Available: <https://kieranwynn.github.io/pyquaternion/>.
- [20] A. Sabatini, C. Martelloni, S. Scapellato, and F. Cavallo, “Assessment of walking features from foot inertial sensing,” *IEEE Transactions on Biomedical Engineering*, vol. 52, no. 3, pp. 486–494, Mar. 2005. DOI: 10.1109/tbme.2004.840727. [Online]. Available: <https://doi.org/10.1109/tbme.2004.840727>.
- [21] J. Perry, *Gait analysis*. Thorofare: SLACK, Jun. 1992, ISBN: 9781556421921.
- [22] J. Mercer, B. Bates, J. Dufek, and A. Hreljac, “Characteristics of shock attenuation during fatigued running,” *Journal of Sports Sciences*, vol. 21, no. 11, pp. 911–919, Nov. 2003. DOI: 10.1080/0264041031000140383. [Online]. Available: <https://doi.org/10.1080/0264041031000140383>.

- [23] J. Zeni, J. Richards, and J. Higginson, “Two simple methods for determining gait events during treadmill and overground walking using kinematic data,” *Gait & Posture*, vol. 27, no. 4, pp. 710–714, May 2008. DOI: 10.1016/j.gaitpost.2007.07.007. [Online]. Available: <https://doi.org/10.1016/j.gaitpost.2007.07.007>.
- [24] L. Vargas-Valencia, A. Elias, E. Rocon, T. Bastos-Filho, and A. Frizera, “An IMU-to-body alignment method applied to human gait analysis,” *Sensors*, vol. 16, no. 12, p. 2090, Dec. 2016. DOI: 10.3390/s16122090. [Online]. Available: <https://doi.org/10.3390/s16122090>.
- [25] X. T. B.V., *Mtw awinda user manual*, English, version Document MW0502P, Revision L, Xsens, May 2018, 88 pp., 3 May 2018.
- [26] J. M. Bland and D. Altman, “STATISTICAL METHODS FOR ASSESSING AGREEMENT BETWEEN TWO METHODS OF CLINICAL MEASUREMENT,” *The Lancet*, vol. 327, no. 8476, pp. 307–310, Feb. 1986. DOI: 10.1016/S0140-6736(86)90837-8. [Online]. Available: [https://doi.org/10.1016/S0140-6736\(86\)90837-8](https://doi.org/10.1016/S0140-6736(86)90837-8).

APPENDIX

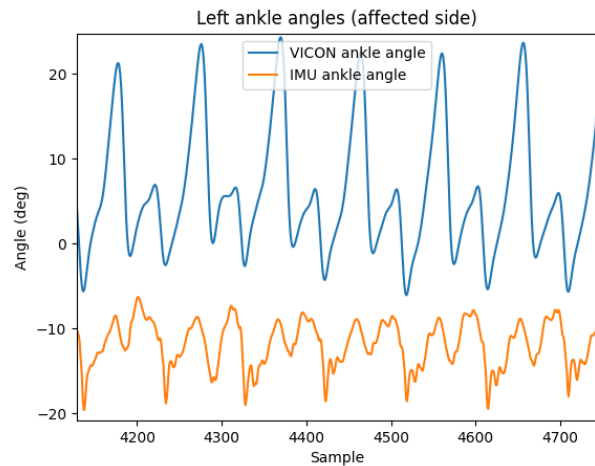


Figure 12: Example time series of the ankle angles when comparing the Vicon and IMU data. The IMU results are determined using the method by Vargas-Valencia [24] as explained in the Methods (Section III).